

# Damage Tolerance Analysis of Repaired Composite Structures: Engineering Approach and Computational Implementation

Mark R. Gurvich, Vijay N. Jagdale

United Technologies Research Center

411 Silver Lane, MS 129-73, East Hartford, CT 06108, USA

[GurvicMR@utrc.utc.com](mailto:GurvicMR@utrc.utc.com), [JagdalVN@utrc.utc.com](mailto:JagdalVN@utrc.utc.com)

*Abstract: This study is focused on analysis of post-repair behavior of composite structures. The objectives are to a) develop efficient computational approach for repaired areas, capturing processes of both damage initiation and growth; and b) demonstrate it in Abaqus on representative examples of composite repair designs. The approach is based on cohesive elements (CE), and the robust nature of generated numerical predictions is shown. Thus, the approach provides a very convenient FEA implementation and, on the other hand, can generate sufficient accuracy for repair-related design and service decisions. Results of parametric studies are presented for selected cases to demonstrate sensitivity of damage tolerance of repaired zones to input parameters (load conditions, geometrical characteristics, repair imperfections, etc.).*

*Keywords: Composites, Repair, Damage, Delamination, Fracture, Failure.*

## 1. Introduction

### 1.1 Importance

Existing modeling capabilities to predict damage tolerance (DT) of composites are primarily applied to *new* untouched components. However, typical composite structures (both defense and commercial) are usually susceptible to numerous damages in operation, transportation, maintenance, etc. Therefore, reliable modeling approaches to understand and quantify DT of repaired composite components and structures could provide significant cost and labor benefits by avoiding expensive component replacement, increasing residual post-repair life, simplifying repair solutions, etc. The problem is that repair-related decisions are still mainly empirical and based primarily on generated field experience, common sense, and understandable over-design conservatism. Available modeling solutions in this area are anecdotal, and their main ideas are briefly discussed below on examples of representative publications.

### 1.2 Literature review

Literature pertaining to analysis of adhesive joints can be extended to the analysis of repaired composite structures assuming all damaged parent material have been removed from the structure before repair layup. Some analytical approaches (Yang *et al.*, 2004; Zhang *et al.*, 2006), amongst others, have been applied to the analysis of adhesively bonded composite joints. But these methods are limited to simple single-lap composite joint geometries (Yang *et al.*, 2004) and they

use linear elastic material behavior for adherends while allowing plastic behavior only for the adhesive layer. Mathematical formulation becomes very complex if material non-linearity due to plastic behavior of adherends is modeled. For complex geometries, the three dimensional nature of problem coupled with material nonlinearities leads to the use of finite element methods for analyzing adhesively bonded joints.

### **1.2.1 Continuum mechanics based approach**

Continuum mechanics based criteria have been used to predict the joint strength. In this approach, the adhesive and adherends are modeled using continuum elements. The adhesive is assumed to be perfectly bonded to the adherends with no account of the adhesion properties of the interface. Maximum stress (Adams *et al.*, 1986; Kumar *et al.*, 2006), strain or plastic energy density is used as failure criterion. Due to the bi-material singularities inherent in a bonded joint, maximum stress or strain based criterion becomes sensitive to mesh refinement and “stress or strain at a distance” approach is sometimes used (Towse *et al.*, 1999). Such approaches have relatively low computational cost, require small number of material properties with relatively simpler material property evaluation and model validation experimental programs but this approach is conservative (e.g. no account of the adhesion properties at the interface) and subjective to analysis at finite size from singularity.

### **1.2.2 Fracture mechanics based approach**

In fracture mechanics based approach, an energy parameter is used as failure criterion, e.g., Hutchinson and Suo (1992) used critical mixed mode energy release rate to predict crack path and the strength of the joint under given loading condition. This approach is subjective to the presence of a crack. Alternatively, generalized stress intensity factor based approach (Gleich *et al.*, 2001) can be utilized to predict joint strength. Such approaches have moderate computational cost. As compared to continuum based approach, in general, much more involved material property determination and experimental model validation program is required.

### **1.2.3 Progressive damage based approach**

Progressive damage modeling approaches are used to capture the complete response of structure up to the final point of the failure in single analysis. In cohesive element based (CE) modeling approach (Kafkalidis and Thouless, 2002; Campilho *et al.*, 2009a; Campilho *et al.*, 2009b; Li *et al.*, 2006; Pinto *et al.*, 2010), the damage is restricted to zero volume lines (two dimensional analysis) or surfaces (three dimensional analysis). A CE simulates damage along a predefined crack path by specifying traction-separation response between initially coincidental nodes on either side of the path. CE models use both strength and energy parameters to characterize the debonding process along the crack path, thus making its application more general than fracture mechanics based approaches. Continuum damage models, where the damage is modeled over a finite region, provide an alternative, when crack path is not known a priori and when adhesive thickness has to be considered (de Moura *et al.*, 2008). Simplification of CE-based modeling approaches for practical engineering applications seems to be the next step.

## **1.3 Objectives**

The objectives of this study are to a) develop engineering computational approach of DT assessment for repaired areas, capturing processes of both damage initiation and growth; and b)

demonstrate its robustness in Abaqus on representative 2D and 3D examples of composite repair designs.

## 2. Concept and Approach

Considered concept is motivated by successful CE-based modeling in recent repair-related works (Pinto *et al.*, 2010; Campilho *et al.*, 2009b). The proposed idea is to simplify CE-based solutions and make them standard design tools for practical engineering analysis. Therefore, successful implementation of this problem should be driven between the Scylla and Charybdis of physical fidelity and computational cost/convenience. The following two simplifying assumptions are proposed here to achieve this goal:

- 1) interfacial properties between connected parts and interlaminar properties between individual layers are considered the weakest links of repair zones.
- 2) structural integrity of repaired zone is controlled by the very worst scenario of damage initiation and growth.

The first assumption allows one to ignore consideration of cross-laminar damage and, more generally, complex damage networks, since interfacial and/or interlaminar damage alone seem to be severe enough for definition of the load limit. The second one provides a convenient opportunity to consider only a few the most dangerous damage paths instead of numerous mathematically possible combinations of damage growth scenarios.

According to the assumptions, the considered approach can be schematically illustrated on example of a double scarf repair (Hexcel, 1999) of sandwich composite structure (Figure 1,a). Here, actual design is simplified as a combination of connected parts (Figure 1,b) including original and repaired (added) components. Next, expected damage scenarios are brain-stormed (Figure 1,c) and defined. The follow-up step (Figure 1,d) is consideration of *all* interfacial and interlaminar surfaces where either damage initiation or growth can be expected in principle. This step can be associated with potentially too complex damage network with high risk of convergence challenges and/or non-unique solutions. Thus, the next step is selection of the most probable *individual* damage paths (e.g., Figures 1,e and 1,f) with their *separate* modeling using CE along the selected damage paths. Finally, modeling results for individual damage cases are compared to select the very worst scenario and to define the limit load.

In addition, potential imperfections of repaired interfacial contacts can be taken into account through introduction of small initial cracks. A more systematic analysis of such imperfections will be considered in the follow-up 2D and 3D examples.

## 3. Computational Implementation

Representative 2D and 3D repair geometries are considered in this study. In 2D analysis of considered example, plane strain analysis is applied. The composite laminate is modeled using plane strain 4-node bilinear quadrilateral elements (CPE4). Mesh convergence study is performed (Section 4.2) to obtain acceptable mesh refinement while balancing the computational cost. In 3D analysis, composite laminate is modeled using 8-node linear brick elements (C3D8). Mesh is

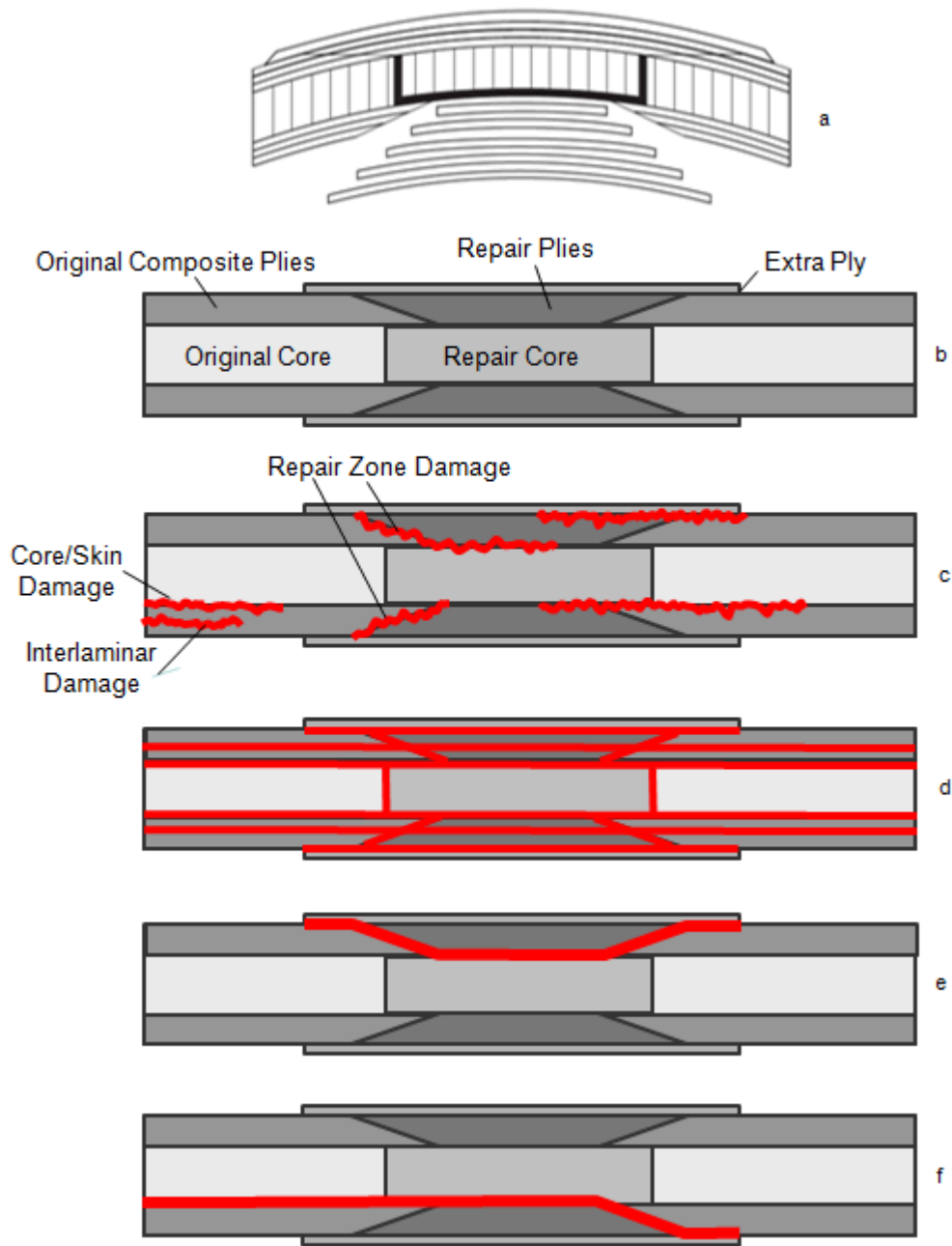


**Figure 1. Schemes of a) repair; b) FEA statement of analysis; c) expected damage scenarios; d) model capturing "all" damage mechanisms; and e), f) examples of models with selected individual paths of damage propagation.**

refined near cohesive zone to improve model accuracy. Analyses are performed in Abaqus/Standard 6.10-1 allowing large scale, nonlinear deformation to occur.

Laminates considered in the work, for demonstration purpose only, are assumed to be made up of unidirectional layup. However, the computational approach can be extended to laminates of any layup of interest, with appropriate identification of damage paths. The individual unidirectional composite plies (Hexcel 8552 IM7 unidirectional prepreg) are modeled as homogeneous anisotropic linear elastic material (Table 1). Displacement controlled load is applied at the end of the laminate. 2D model is analyzed for tensile as well as bending displacement controlled loading while 3D model is analyzed for tensile loading only.

**Table 1. Laminate ply mechanical properties (Hexcel, 2011).**

$E_1 = 158.511$ GPa	$\nu_{12} = 0.316$	$G_{12} = 4.688$ GPa
$E_2 = 8.963$ GPa	$\nu_{13} = 0.316$	$G_{13} = 4.688$ GPa
$E_3 = 8.963$ GPa	$\nu_{23} = 0.380$	$G_{23} = 3.247$ GPa

In 2D analysis, 4-node 2D CEs (COH2D4) are utilized to define adhesive bondline cohesive layer as well as interlaminar cohesive layers. In 3D analysis, 8-node 3D CEs (COH3D8) are used to model the adhesive bondline cohesive zone. CEs with triangular traction-separation response are utilized (Abaqus, 2010). Damage initiation is modeled using quadratic nominal stress criterion ( $S = 64.1$  N/mm<sup>2</sup>;  $T = 91.1$  N/mm<sup>2</sup>). Damage evolution is defined based on fracture energy with linear softening and BK mix-mode behavior at  $G_{IC} = 0.1751$  N/mm;  $G_{IIC} = 0.7005$  N/mm;  $\eta = 2.5$ . For demonstration purpose, in 2D analysis, both adhesive bondline and interlaminar cohesive layers are assumed to have same CE properties.

## 4. 2D Example

### 4.1 Problem Statement

The geometry of the scarf repair, considered for demonstration, is shown in Figure 2. Selection of this example was motivated by work of Campilho *et al.*, 2009b. The  $[0]_{20}$  laminate is 115 mm long, 25.4 mm wide and 3.81 mm thick. To reduce the model size, the scarf repair patch is treated as a rigid body adhesively bonded to the composite laminate. This is considered to provide conservative and representative failure initiation load values. Any possible failure modes of repair patch are thus not considered in the analysis. For different scarf angles, minimum laminate length of 30 mm is considered during the analysis. The specimen is idealized as a 2D geometry analyzed under plane strain condition. To achieve reliable results, a refined mesh is utilized as shown in Figure 2,d. The following possible imperfections and damage mechanisms are identified (Figure 2,e) :

- 1) Case A : An imperfection is created at the bottom part of the adhesive bondline, which propagates to cause complete adhesive bondline failure (debonding).
- 2) Case B : An imperfection at the top side of the adhesive bondline, propagating with increased load causing debonding.
- 3) Case C : Interlaminar defect/crack near the adhesive bondline at the mid-surface of the laminate, which propagates along the laminate mid-surface away from the adhesive bondline resulting in failure of laminate.

- 4) Case *D* : Extension of Case *C*, where initial imperfection is observed at each interlaminar layer near the adhesive bondline.

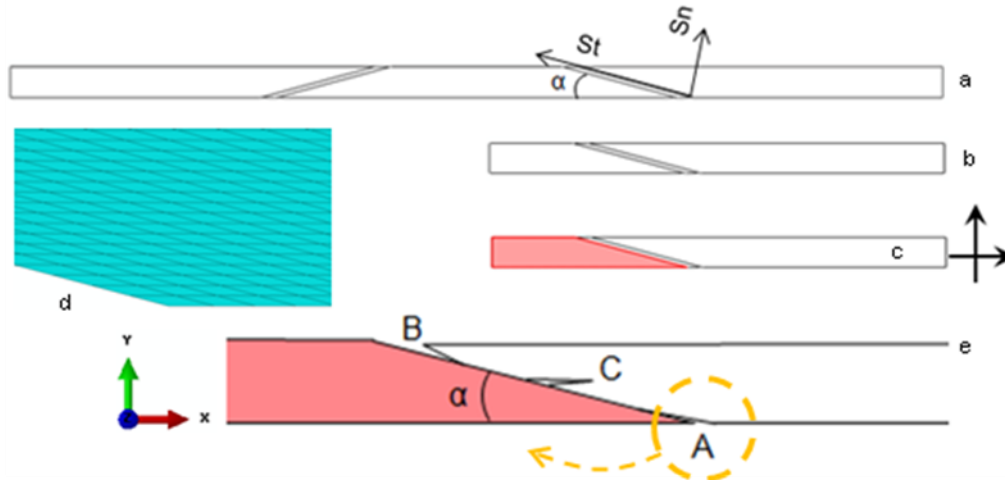


**Figure 2.** 2D scheme of a) scarf repair, b) its symmetric model, c) definition of load d) fragment of FEA mesh around crack A ; and e) damage mechanisms.

Each damage case is isolated and analyzed separately. Results for individual case are then considered together to identify a critical failure initiation location. Additionally, effect of initial size of imperfections ( $a/W$  ratio) is studied for different scarf angles ( $\alpha = 15^\circ, 30^\circ, 45^\circ$ ). Initial  $a/W$  ratio is reported as a fraction of the adhesive bondline length for case A and B or thickness of the laminate for case C and D. The words case, crack, crack location and imperfection location are used interchangeably in the text.

#### 4.2 Effect of mesh density

Effect of mesh density is analyzed for case A subjected to the bending displacement-controlled loading at  $a/W = 0.25$ . Table 2 summarizes the convergence results with  $m_y$  and  $m_x$  representing number of elements in thickness and laminate length direction, respectively. The reported  $P_{max}$  value (in N/mm) corresponds to the load value when failure is initiated near the imperfection A. Reported % values are calculated by considering most refined mesh as a reference ( $P_{max} = 128$  N/mm, wallclock time = 64.2 mins).  $P_{max}$  results are found to converge with increased mesh density. Mesh with  $m_y = 100$  and  $m_x = 200$ , provides a good tradeoff between model accuracy and computational cost. This mesh is utilized for further analysis.

**Table 2.** Mesh convergence study results.

$m_y$	$m_x$	Total elements	Error in $P_{max}$ prediction (%)	Computational time (%)
20	40	800	35.86	0.3
40	80	3,200	11.25	1.5
80	160	12,800	2.89	29.4
100	200	20,000	1.72	45.1
160	320	51,200	0.39	62.0
200	400	80,000	0.00	100.0

### 4.3 Solution stabilization

Use of adaptive automatic stabilization is explored for improving model convergence after failure is initiated in the laminate or adhesive bondline. Corresponding input file lines in the step definition are provided below:

`*Static, stabilize = dissipated energy fraction, allsdtol = accuracy tolerance`

Dissipated energy fraction of 0.0002 and accuracy tolerance of 0.05 is used in the study. Model setup without such stabilization scheme is observed to predict same failure initiation displacement ( $\delta_{max}$ ) value while predicting practically same failure initiation load,  $P_{max}$  for different initial imperfection locations at fraction of the computational cost (Table 3 and Figure 3). Reported results, in the next sections, thus do not make use of any solution stabilization scheme. However problems with more complex geometries and failure propagation scenarios can benefit from such solution stabilization.

**Table 3. Results with and without use of adaptive automatic stabilization.**

Case	Force and displacement results				Time (min)		
	$P_{max}$ with stabilization (N/mm)	$P_{max}$ without stabilization (N/mm)	$\Delta P_{max}$ (%)	$\delta_{max}$ (mm)	with stabilization	without stabilization	ratio
A	11,481	11,487	0.052	0.0318	33.80	6.42	5.3
B	16,995	17,003	0.047	0.0418	3.83	3.55	1.1
C	143,740	143,740	0	0.3294	29.47	11.02	2.7

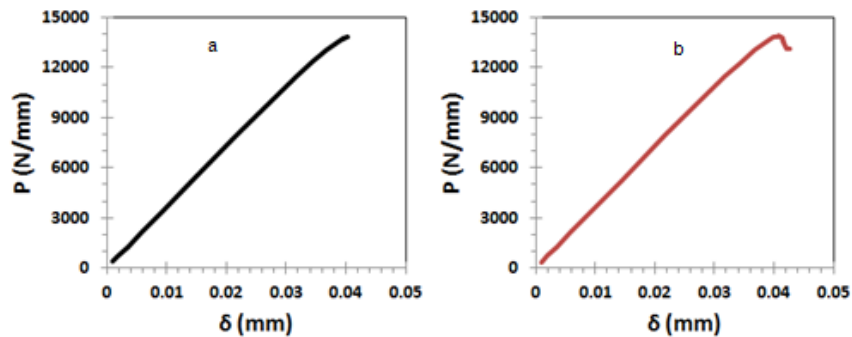


**Figure 3. Deformation diagrams a) without and b) with stabilization for case A.**

### 4.4 2D parametric results

Since large number of cases are analyzed (two loading conditions, three scarf angles, four initial imperfection locations and five initial crack sizes), a Matlab® code is developed inhouse to automate the input file generation and preliminary result analysis.

For the current problem definition, analysis of the strain distribution in the laminate will provide an insight into the behavior of cohesive zones. Figure 4 provides the shear strain distribution for 15° scarf angle laminate under tensile displacement loading. Maximum crack size of  $a/W = 0.25$

and same value of displacement is used in the results, for demonstration. Under tensile loading, the presence of initial crack in the adhesive cohesive layer (crack *A* or *B*) results in high strain regions close to the discontinuity, while interlaminar cracks *C* and *D* do not adversely affect the strain distribution in the laminate. Tensile displacement controlled loading will create high normal strains ( $\epsilon_{xx}$ ) in the bottom region of the scarf repair (close to crack *A* location), which combined with high shear strains in the laminate will cause high strains and stresses in the adhesive bondline CEs leading to its failure. At the chosen tensile displacement value, crack *A* has already initiated failure in the adhesive cohesive layer, thus indicating it is a critical failure initiation location, amongst the failure mechanisms considered here, for the tensile displacement controlled loading.

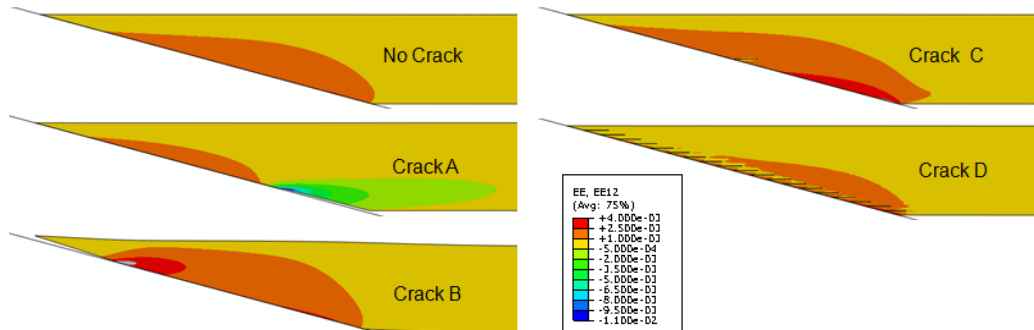


**Figure 4. Distribution of shear strain,  $\epsilon_{xy}$  for different damage mechanisms under tensile displacement,  $\delta = 0.03178$  mm ( $\alpha = 15$  deg).**

Similar observations are made for the case with tip bending displacement load (refer Figure 5). Under such a loading bottom point of the scarf repair will have high normal bending strains, which couple with high shear strains in the laminate caused by crack *A* to initiate failure in the adhesive bondline CEs. The strains and stresses in the adhesive bondline cohesive layer follow the trend of the strains and stresses in the laminate especially at lower scarf angles and in the presence of initial imperfections. The shear strains near the crack tip are higher for crack *A* than crack *B*. Presence of interlaminar crack near bottom portion (between first and second composite ply), in case *D*, makes it prone to early failure, as will be shown in subsequent results.

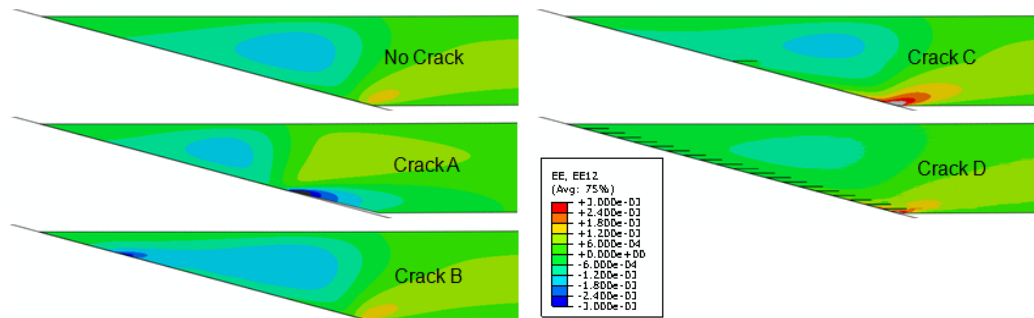


**Figure 5. Distribution of shear strain,  $\epsilon_{xy}$  for different damage mechanisms under bending displacement  $\delta = 0.2128$  mm ( $\alpha = 15$  deg,  $a/W = 0.25$ ).**



Effect of scarf angle on strain distribution under tensile displacement controlled loading is shown in Figure 6. The strain distributions are shown at individual failure loads. As can be deduced, for crack A, the failure displacements and loads reduce as the scarf angle increases (also shown in Figure 8). The peel stress increases as the scarf angle increases. Owing to the lower peel strength as compared shear strength of adhesive, the failure is observed to initiate earlier, as we increase the scarf angle. The presence of initial imperfections acts as strain and stress riser, initiating debonding.

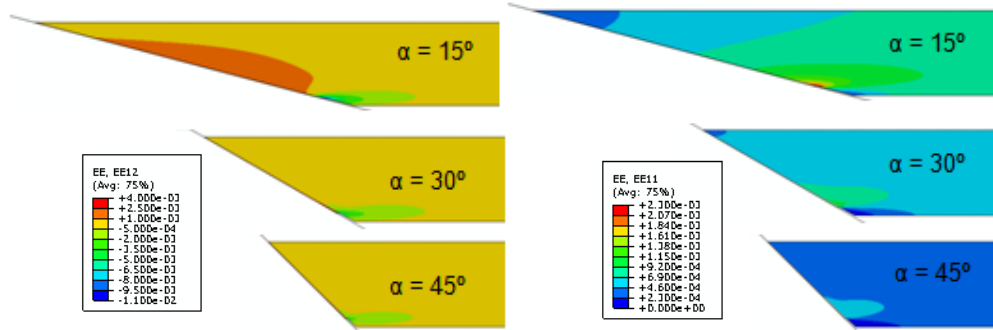


**Figure 6. Effect of scarf angle on strain distributions for crack A under tensile load ( $a/W = 0.1$ ).**

Effect of initial crack location and size on failure load is shown in Figure 7. As can be seen and discussed earlier crack location A is critical for both the loading types, considered here, and will determine the load carrying capacity of the repaired laminate. It is checked that the failure strength of the  $0^\circ$  plies is not attained before the repair patch debonding onset, due to crack A. For tensile displacement load condition and crack A, as compared to a quality bond ( $a/W = 0$ ), the failure initiation load is observed to reduce by 25% for  $a/W = 0.05$  and by 33.5% for  $a/W = 0.25$ . The reduction is observed to be more severe for crack location B alone (by 57% for  $a/W = 0.05$  and by 84% for  $a/W = 0.25$ ). For tensile loading condition crack C and D are not of a concern. For bending load, crack D becomes more critical as compared to crack location B. Crack A still determines the repair strength. Such results can be used to calculate safety margins based on presence of expected damage mechanisms.

With increase in scarf angle the repair strength is observed to reduce for both tensile and bending loading conditions (Figure 8). For tensile loading case, the repair strength is observed to reduce by 27% as the scarf angle is increased from  $15^\circ$  to  $30^\circ$  and by 52% for change in scarf angle from  $15^\circ$  to  $45^\circ$ . For bending loading case these reductions are by 25% and 42% respectively. The % reduction in strength is observed to maintain its trend more or less same with increase in initial crack size. Results highlight the importance of using lower scarf angles for composite repairs in order to maximize the repair strength. Additional improvements in repair design to avoid or delay damage mechanism A would beneficially help increase the repair strength.

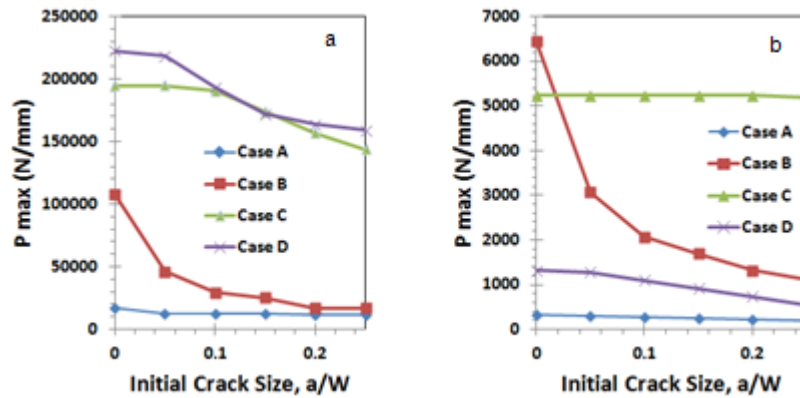


Figure 7. Effect of initial crack location and size on failure load for tensile displacement load (a) and bending displacement load (b).

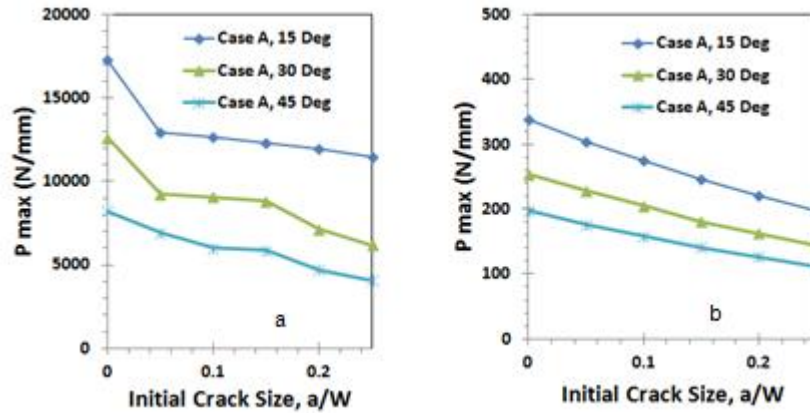


Figure 8. Effect of scarf angle on failure load for tensile displacement load (a) and bending displacement load (b) for crack A.

## 5. 3D Example

### 5.1 Problem Statement

The geometry of the laminate with a circular scarf repair, considered for demonstration, is shown in Figure 9,a. It corresponds to a repair procedure where a laminate has undergone damage due to a projectile. The  $[0]_{20}$  laminate is 120 mm long, 120 mm wide and 3.81 mm thick. The damaged region is removed, for example, by grinding the damaged material with a scarf shape. A repair patch with complimentary shape of removed material is bonded to the parent material. The scarf shape, considered in analysis, has one inch (25.4 mm) diameter hole in the base with a representative 30 deg scarf angle. The periodic segment considered in the analysis is shown in Figure 9,b. Due to the circular scarf shape the stress state is particularly multi-axial in nature

requiring three dimensional analysis. The mesh is refined near the scarf region, with 60 elements along  $S_r$  co-ordinate direction and 90 elements for  $1/4^{\text{th}}$  of the cohesive zone in the radial direction. As done in the earlier 2D analysis, the scarf repair patch is treated as a rigid body adhesively bonded to the composite laminate. The repaired composite is analyzed under tensile displacement controlled load applied at the tip of the laminate. Effect of initial size of the imperfection located at the top portion of the cohesive zone (corresponding to Case A in 2D analysis) is explored.  $a/W$  ratio of 0.05, 0.15 and 0.25 is used in the present study.

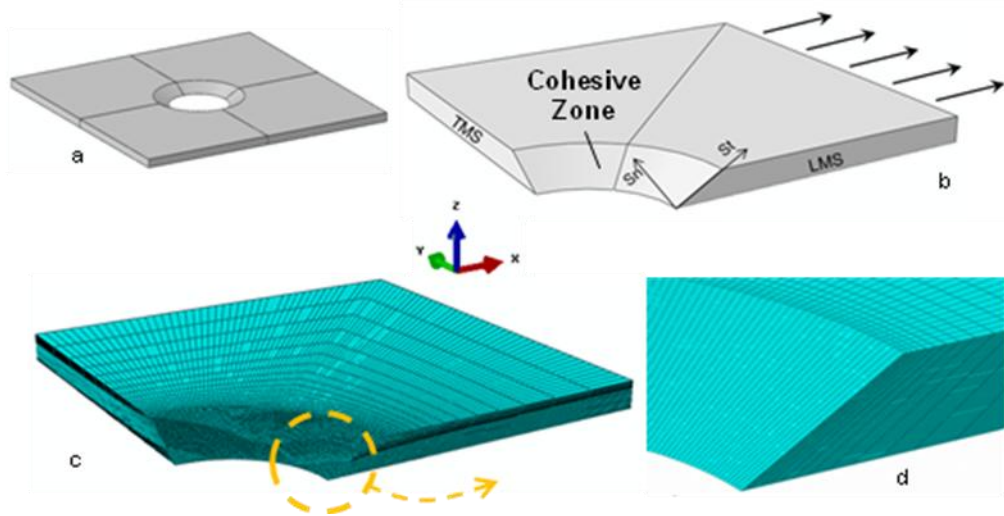


**Figure 9. Full geometry (a) and considered periodic segment (b); FEA mesh (c) and its detail (d).**

## 5.2 Results

### 5.2.1 Stress and failure analysis in cohesive zone at $a/W = 0$

Figure 10 shows the distribution of stresses and damage parameters in the cohesive zone at the failure initiation point, as seen from the top. Material direction 3 is in the CE thickness direction computed based on the midsurface of the CEs. Directions 1 and 2 are in global  $X-Z$  and  $Y-Z$  plane respectively. Due to the applied tensile displacement controlled load in longitudinal direction, stresses  $S_{33}$  and  $S_{13}$  are observed to dominate stress  $S_{23}$ . Both the  $S_{33}$  and  $S_{13}$  stresses are observed to be higher in the cohesive zone near the top portion of the scarf region on longitudinal middle surface (LMS) plane. These stresses are observed to reduce as we move from LMS plane to transverse middle surface (TMS) plane and from top to the bottom portion of the scarf repair. Failure initiation is evidenced by the fact that the quadratic nominal stress criterion (QUADSCRT) has approached 1 in this region and the scalar stiffness degradation parameter (SDEG) has a value of greater than 0. No stable crack growth is predicted. Numerical prediction terminated abruptly once the crack started to propagate. If energy stored by the specimen exceeds the energy required to fracture the remaining adhesive bondline, it will lead to a catastrophic failure, as one predicted here. Distribution of QUADSCRT provides the information of the potential crack propagation direction, indicating crack will propagate simultaneously in the radial direction at the top of the

cohesive zone and from top to the bottom portion at the LMS plane. Figure 11 shows the evolution of QUADSCRT as the tensile load increases to failure load value. Gradual increase in QUADSCRT at failure initiation location is evident.

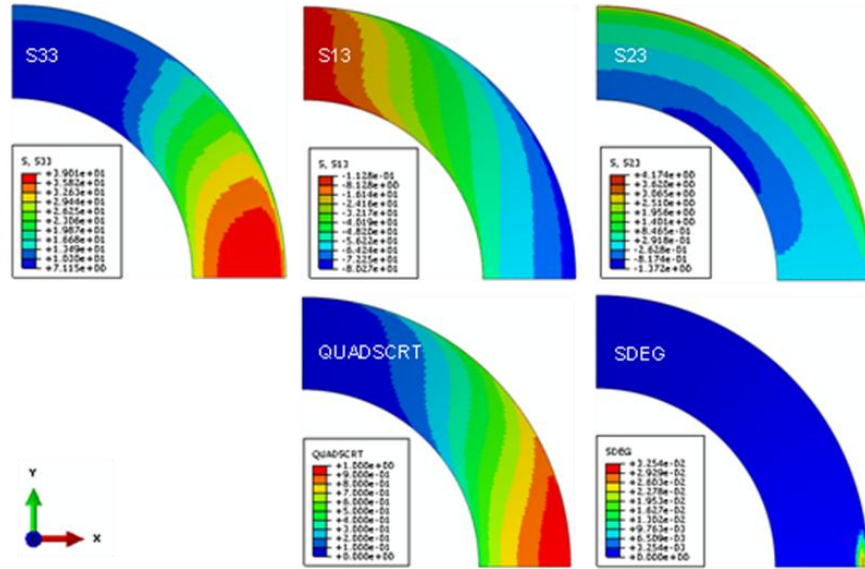


Figure 10. Distribution of stresses and damage parameters in cohesive zone.

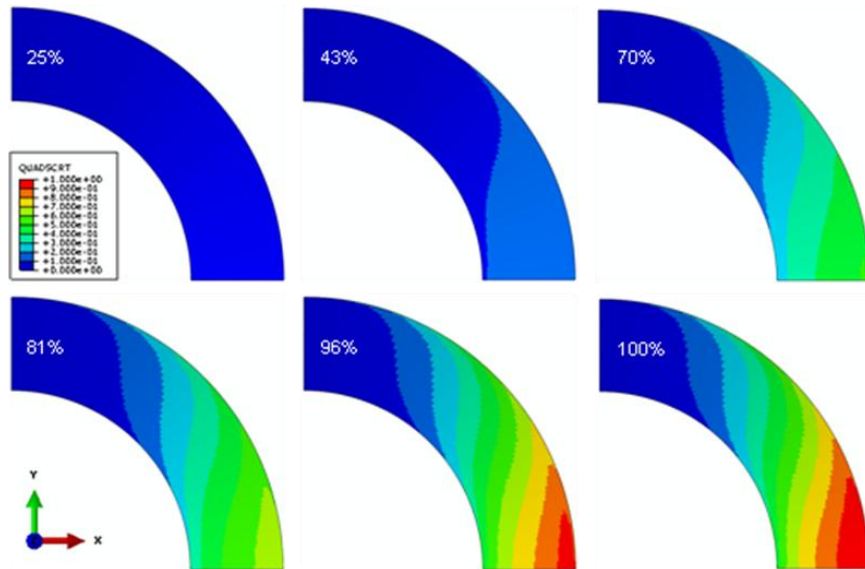


Figure 11. Distribution of QUADSCRT as function of failure load (%) at  $a/W = 0$ .

### 5.2.2 Effect of initial imperfections

Initial imperfections of varying size ( $a/W = 0.05, 0.15$  and  $0.25$ ) are introduced near the top edge of the cohesive zone and its effect on the load displacement curve and failure initiation load is studied. As can be seen in Figure 12, the gradient in QUADSCRT is found to be steeper near LMS plane and at various radial planes along the cohesive zone, as the initial imperfection size increases. This is the indication of an increased stress concentration in such cases near the crack tip with higher initial crack size. As the initial imperfection size increases, damage is observed to occur instantaneously in a greater radial region (Figure 13). Numerical procedure is observed to terminate abruptly as the crack starts to propagate owing to expected catastrophic failure, as discussed earlier.

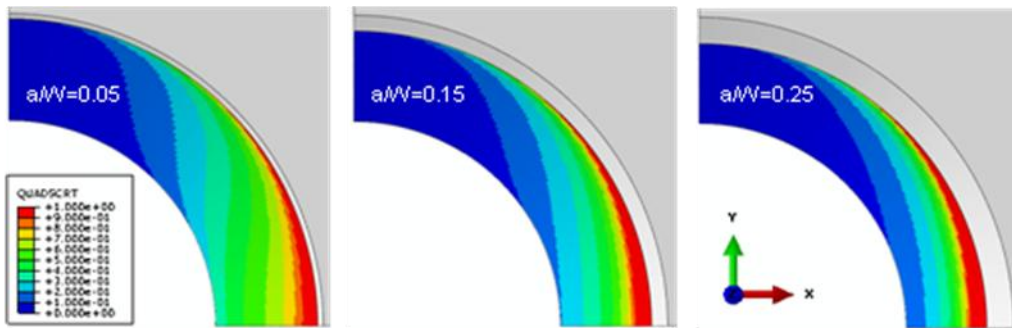


Figure 12. Effect of initial crack on QUADSCRT distribution (100% failure load).

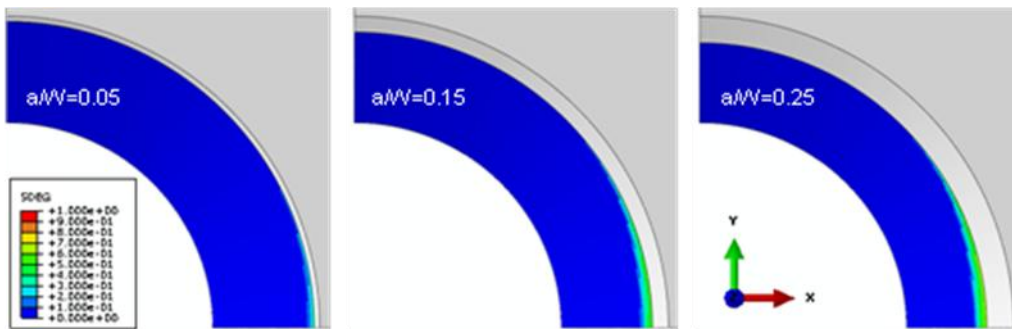


Figure 13. Effect of initial crack on SDEG distribution (100% failure load).

With the increase in size of initial imperfection, stiffness of the repaired structure is observed to reduce owing to resultant smaller effective area supporting the tensile load (Figure 14). Force-displacement response is linear till adhesive bondline failure. It is checked that the failure strength of the  $0^\circ$  plies is not attained before the repair patch debonding onset. Failure load reduces by 19% when  $a/W = 0.05$ , by 36% for  $a/W = 0.15$  and by almost 49% for the case with  $a/W = 0.25$ . These

representative quantities highlight the importance of manufacturing process quality control and accurate methods for inspection and quantification of any initial imperfections that might be present in the scarf repaired composites caused during the manufacturing process.

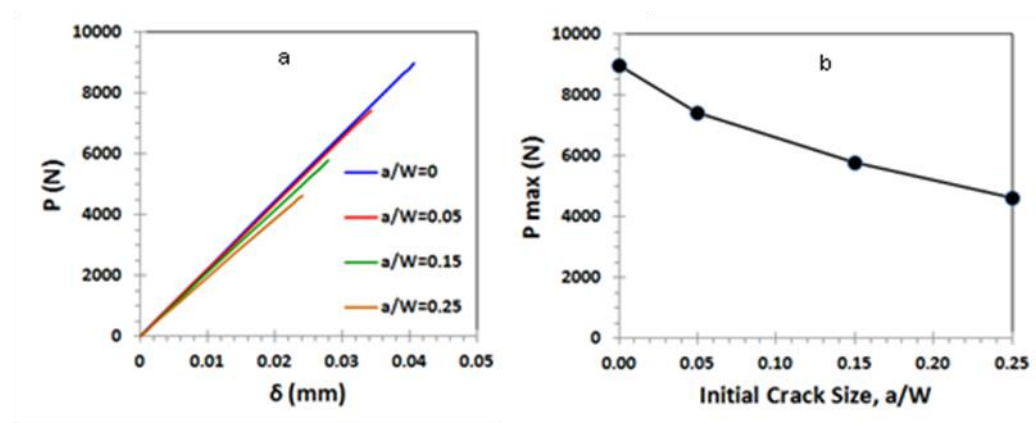


Figure 14. Force-displacement diagrams (a) and max loads (b) as functions of initial crack size  $a/W$ .

## 6. Conclusions

A convenient engineering approach is suggested and demonstrated for DT assessment of repaired zones in composite structures. Efficient FEA implementation of the approach is achieved through robust Abaqus capabilities to model damage initiation and growth by CEs. It is shown that limit loads can be predicted relatively easy by analysis of several major expected damage paths and follow-up selection of the worst case scenario. In addition, repair imperfections can be taken into account through initial suggested cracks, and generated results can be potentially used for analysis of safety margins. Successful application of the approach is demonstrated for both 2D and 3D statements of analysis, and therefore, can be suggested for analysis and optimization of a wide range of repair designs. The follow-up efforts are focused on experimental validation of the approach and its expansion for fatigue life analysis.

## 7. References

1. Abaqus Analysis User's Manual, 2010, Dassault Systemes Simulia Corp., Providence, RI, USA.
2. Adams, R. D., Atkins, R. W., Harris, J. A., and Kinloch, A. J., "Stress Analysis and Failure Properties of Carbon-Fibre-Reinforced-Plastic/Steel Double-Lap Joints," *Journal of Adhesion*, 20 (1986), pp. 29–53.
3. Campilho R.D.S.G., de Moura M.F.S.F., Ramantani D.A., Morais J.J.L., and Domingues J.J.M.S., "Tensile Behaviour of Three-Dimensional Carbon-Epoxy Adhesively-Bonded Single and Double-Strap Repairs," *International Journal of Adhesion & Adhesives*, 29 (2009a), pp. 678–686.

4. Campilho R.D.S.G., de Moura M.F.S.F., Pinto A.M.G., Morais J.J.L., and Domingues J.J.M.S., “Modelling the Tensile Fracture Behaviour of CFRP Scarf Repairs,” *Composites:Part B – Engineering* 40 (2009b), pp. 149–57.
5. de Moura, M. F. S. F., Gonçalves, J. P. M., Chousal, J. A. G., and Campilho, R. D. S. G., “Cohesive and Continuum Mixed-Mode Damage Models Applied to the Simulation of The Mechanical Behaviour of Bonded Joints,” *International Journal of Adhesion & Adhesives*, 28 (2008), pp. 419–426.
6. Gleich, D. M., Van Tooren, M. J. L., and Beukers, A., “Analysis and Evaluation of Bondline Thickness Effects on Failure Load in Adhesively Bonded Structures,” *Journal of Adhesion Science and Technology*, 15 (2001), pp. 1091–1101.
7. Hutchinson, J. W. and Suo, Z., “Mixed-Mode Cracking in Layered Materials,” *Advances in Applied Mechanics*, 29 (1992), pp. 63–191.
8. Hexcel Composites, “Composite Repair,” Publication No. UTC 102, April 1999.
9. “Hexcel 8552 IM7 Unidirectional Prepreg 190 gsm & 35% RC Qualification Material Property Data Report,” National Institute for Aviation Research, Test Report Number CAM-RP-2009-015 Rev A, April 22, 2011.
10. Kafkalidis, M.S., and Thouless, M.D., “The Effects of Geometry and Material Properties on the Fracture of Single Lap-Shear Joints,” *International Journal of Solids and Structures*, 39 (2002), pp. 4367–4383.
11. Kumar S.B., Sridhar I., Sivashanker S., Osiyemi S.O., and Bag A., “Tensile Failure of Adhesively Bonded CFRP Composite Scarf Joints,” *Materials Science and Engineering B*, 132 (2006), pp. 113–20.
12. Li, S., Thouless, M., Waas, A., Schroeder, J., and Zavattieri, P., “Competing Failure Mechanisms in Mixed-Mode Fracture of an Adhesively Bonded Polymer–Matrix Composite,” *International Journal of Adhesion & Adhesives*, 26 (2006), pp. 609–616.
13. Pinto A.M.G., Campilho R.D.S.G., de Moura M.F.S.F., and Mendes I.R., “Numerical Evaluation of Three-Dimensional Scarf Repairs in Carbon-Epoxy Structures,” *International Journal of Adhesion & Adhesives*, 30 (2010), pp. 329–337.
14. Towse, A., Potter, K. D., Wisnom, M. R., and Adams, R. D., “The Sensitivity of a Weibull Failure Criterion to Singularity Strength and Local Geometry Variations,” *International Journal of Adhesion and Adhesives*, 19 (1999), pp. 71–82.
15. Yang, C., Huang, H., Tomblin, J. S., and Sun, W., “Elastic–Plastic Model of Adhesive-Bonded Single-Lap Composite Joints,” *Journal of Composite Materials*, 38 (2004), pp. 293–309.
16. Zhang, J., Bednarczyk, B. A., Collier, C., Yarrington, P., Bansal, Y., and Pindera, M. J., “Analysis Tools for Adhesively Bonded Composite Joints, Part 2: Unified Analytical Theory,” *AIAA Journal*, 44 (2006), pp. 1709–1719.

## 8. Acknowledgements

The authors thank the United Technologies Research Center for permission to publish this paper.